Morphological and imaging evaluation of the metacarpophalangeal and metatarsophalangeal joints in healthy and lame donkeys.

Samir A.A. El-Gendy[a*], Mohamed A.M. Alsafy[a], Catrin Sian Rutland[b*], Ahmad N. EL-Khamary[c], Howaida M. Abu-Ahmed[d] and Mahmoud H. El-Kammar[d]

[a]Department of Anatomy and Embryology, Faculty of Veterinary Medicine, Alexandria University, Egypt.
[b]School of Veterinary Medicine and Science, Faculty of Medicine, University of Nottingham, UK.
[c]Department of Surgery, Faculty of Veterinary Medicine, Damanhur University, Egypt
[d]Department of Surgery, Faculty of Veterinary Medicine, Alexandria University, Egypt
*Corresponding authors: elgendyanatomist@yahoo.com and catrin.rutland@nottingham.ac.uk

elgendyanatomist@yahoo.com Dr. Samir E-Gendy.
safy73@yahoo.com Dr. Mohamed Alsafy
Catrin.rutland@nottingham.ac.uk Dr. Catrin Rutland
ahmed.nasr@damanhour.edu.eg Dr. Ahmad El-Khamary
Howaida_maf@yahoo.com Dr. Howida Abou-Ahmed
m_elkammar2010@yahoo.com Dr. Mahmoud El-Kammar

Highlights

Anatomical description of donkey metacarpophalangeal and metatarsophalangeal joints
Pathologies observed in clinically abnormal donkey joints including exostosis
New anatomical structures observed in donkey joints
Optimized computed tomography methodology can give better visualization for soft tissues

Abstract

The donkey is of socio-economic value yet imaging techniques in both healthy and abnormal limbs are a limiting factor in research and medicine. The objective was to determine anatomical features of both healthy and clinically abnormal donkey metacarpophalangeal and metatarsophalangeal joints (n=13) using anatomical dissection, casting, x-ray and computed tomography. The joint capsule contained two palmar/plantar and two dorsal recesses. The proximal-palmar or plantar recess was larger than the distodorsal recess and potential sites of approaches to the recesses were determined. Soft tissue structures were distinguished using computed tomography at 300mA which was superior to 120mA. This methodology gave better assessments of the synovial tendon sheath, joint recesses and cruciate, collateral and short sesamoidean ligaments. Computed tomography provided outstanding discrimination between the cortex and medulla of the third metacarpal, the proximal sesamoid bones, the proximal phalanx and excellent details of the osseous structures. Although the joints appeared free from exostosis using x-ray; the position and extension of exostosis in pathologically affected donkeys (a novel finding) was revealed using computed tomography with 300mA in comparison to 120mA. The study also provided an anatomical record of the metacarpophalangeal and metatarsophalangeal joints using the latest technology which could impact on clinical situations including anesthesia injection sites.

Keywords:

Computed tomography; Radiography; Exostosis; Lameness.

1. Introduction

The metacarpophalangeal and metatarsophalangeal joints (fetlock joint) have received considerable critical attention because of their anatomical complexity and are the joints most frequently affected by degenerative and traumatic lesions in the equine species [1, 2] causing a high incidence of lameness. Therefore understanding their anatomy and identifying these problems is essential. Current imaging techniques have their limitations in relation to viewing the joint. In cases such as early cartilage loss and subchondral bone injury, radiography and scintigraphy are not always able to detect changes, especially in cases without marked structural bone damage or demineralization. In contrast, evaluation of bone lesions and joint structures may be more appropriate using computed tomography as it provides 3-dimensional images, attenuation coefficient values through windows and tissue density in Hounsfield units [1, 3-6]. Computed tomography can also be useful in understanding orthopedic diseases, during pre-surgical planning and in disease progression prevention. On the other hand soft tissue evaluation with CT can be improved with the use of contrast agents but is often considered inferior to magnetic resonance imaging [6]. It has been demonstrated [7] that using higher tube currents and voltages and thicker sections significantly enhances the accuracy of detection of low-contrast objects. Therefore, it is essential to optimize the factors that could improve image quality in both clinical and research settings to ensure that artifacts and lesions are correctly identified and interpreted.

Donkeys are the tenth most numerous domesticated mammals in the world [8, 9], with an estimated 41 million donkeys supporting 600 million people worldwide [10, 11]. The present study describes the main anatomical structures of the donkey metacarpophalangeal and metatarsophalangeal joints. The hypothesis was that computed tomography undertaken at a high mA would give better images than a lower mA in relation to the metacarpophalangeal and metatarsophalangeal joint, especially when visualizing soft tissue structures. Comparisons between x-rays and computed tomography were also made. The second hypothesis was that limbs from lame animals would show differing anatomical structures when compared to healthy limbs. The third hypothesis was that the anatomical sturctures of the donkey would not differ from those of the horse. The donkey is good for studying equine pathophysiological orthopedic processes, because of its very close phylogenetically, biomechanically and biochemically properties in comparison with the horse [12-14] therefore differences in comparison to the published anatomy of the horse are also discussed. The study also identified new bone growth and pathologies in donkeys with metacarpophalangeal and metatarsophalangeal joint problems. This study presents valuable, clinically relevant, information for anatomical training and research, anesthesia, medicine, surgery in this important animal which is relevant in other animals including the horse.

2. Material and Methods

2.1 Animals and ethics

All four limbs from thirteen adult donkeys of both sexes were used with age matched controls (aged 5-8 years, Table 1). Nomenclature observes Nomina Anatomica Veterinaria terminology [15]. Each donkey (n=13) and their corresponding health records were independently assessed by two specialist donkey and equine lameness veterinary surgeons who confirmed ‘healthy’ or ‘non-healthy’ metacarpophalangeal and metatarsophalangeal joints (Table 1). The following criteria were used: Non-healthy animals had a history of metacarpophalangeal/metatarsophalangeal joint trauma and lameness, which was chronic at the time of investigation with light to moderate (grades 1-2) degrees of lameness which increased after trotting. Animals suspected to have joint effusion with synovial proliferation and osteoarthritic changes based on manual examination (inspection, palpation, passive movement of joints) were also considered ‘non-healthy’. ‘Healthy’ donkeys required a life history and veterinary examination free from deformities/lameness/trauma and study scans further confirmed each diagnosis.

This study followed the guidelines for the care and use of animals and approved by the Animal Welfare and Ethics Committees of the Alexandria University, Damanhur University and The University of Nottingham (ethical number 2173 171214). No animals were euthanized specifically for research purposes. Euthanasia was undertaken under general anesthesia by veterinary surgeons via intravenous injection of 10mg/kg thiopental sodium (EPICO, Egypt) after premedication with 1mg/kg xylazine hydrochloride (Xylaject; Egypt).

2.2 Study Design

2.2.1 Anatomical dissection and cast

Four male and female clinically healthy donkeys free from joint pathology were used. Following euthanasia the animals were bled from the common carotid artery. Metacarpophalangeal and metatarsophalangeal joints from each animal were used (one left forelimb and one right hind limb per animal). The joint cavity of one limb was injected with gum milk latex (Sudan) mixed with a red dye (Carmine Alum Lake, USA) before dissection. One donkey (one metacarpophalangeal and one metatarsophalangeal joint) underwent routine preservative and fixation techniques (10% formalin:4% glycerin:1% phenol; two weeks) prior to dissection. These techniques provided gross anatomical specimens to compliment imaging techniques (Fig. 1+ 4).

2.2.2 Computed radiography

Five healthy and five non-healthy donkeys with chronic joint pathology underwent computed radiography (Table 1). Furthermore, one donkey joint was injected with contrast medium via the palmar recess to further investigate the palmar/plantar recesses. Images were captured on a phosphor plate using Toshiba 500MA fixed x-ray machine, output of 60Kv and 10mA. The time was adjusted automatically with the mA, images were digitally processed using a CR reader (R30-X. Agfa, Japan). Five standard radiographic views were used for each joint, (dorsopalmar, lateromedial, flexed lateromedial, dorso45ºlateral-palmaromedial oblique, and dorsomedial-palmarolateral oblique views with an angle of 45°).

2.2.3 Computed tomography

Five donkeys with joint pathology and two healthy donkeys, all previously used for radiography, were euthanized and the limbs severed at carpal/tarsal joints. Computed tomography protocols (multislice helical computed tomography scanner, Toshiba Astesion Super 4 Edition) were used to obtain 1mm thick scan slices at currents of 120kV and 120mA (lower mA) and 300mA (higher mA). Collimation was at 0.75mm with 4mm reconstruction interval, 1 second rotation time, field of view of 32cm and a pitch of 1.05-2. The matrix size was 512×512 pixels. Both bone (window width 3000, window level 700) and soft tissue (window width 300, window level 80) windows were used. Limbs were placed in the gantry with the long axis of the limb parallel to the table. Limbs were scanned in a distal to proximal direction beginning from proximal aspect of first phalanx and continuing to 2cm above the distal aspect of third metacarpal bone. Specimens underwent bone and soft tissue windows scanning in transverse, sagittal and dorsal planes.

3. Results

3.1 Gross anatomy of the metacarpophalangeal and metatarsophalangeal joints

The articular surfaces of the metacarpophalangeal and metatarsophalangeal joints were comprised of the third metacarpal/metatarsal bone, the proximal phalanx and the paired proximal sesamoid bones. The distal epiphysis of the third metacarpal/metatarsal bone consisted of two condyles separated by a sagittal ridge; the medial condyle was the largest (Figs.2+5+Supplemental Figure 1). The proximal extremity of the proximal phalanx consisted of two articular cavities, the medial cavity slightly larger than the lateral one (Fig.2). The two proximal sesamoid bones had a three sided pyramid shape, their dorsal surfaces articulated with the condyles of the large metacarpal/metatarsal bone (Figs.1+2).

The ligaments of the metacarpophalangeal and metatarsophalangeal joints were the collateral ligaments and sesamoidean apparatus. The medial and lateral collateral ligaments had superficial and deep parts (Fig.1). The sesamoidean apparatus included the suspensory, collateral, straight, oblique, short and cruciate sesamoidean, and intersesamoidean ligaments. The suspensory ligament presented on the palmar surface of the large metacarpal bone between the two splint bones (Fig.1). The suspensory ligament divided into two diverging branches attached to the abaxial surface of the corresponding proximal sesamoid bone. Then the extensor branch of suspensory ligament passed obliquely distally and dorsally to the dorsal surface of the proximal phalanx, where it attached to the common digital extensor tendon or long digital extensor tendon in the hind llimb (Fig.1). The lateral and medial collateral sesamoidean ligaments united the proximal sesamoid bones to the metacarpus proximally and to the proximal phalanx distally (Fig.1). The straight sesamoidean ligament originated from the proximal sesamoid bones and inserted on the palmar border of the base of the proximal phalanx and to the tuberositas flexoria of the second phalanx (Fig.1) covered on the plantar or palmar side by the superficial and deep digital flexor tendon and related tendon sheath. The oblique sesamoidean ligament was narrow in width proximally, wider distally, originating from the base of the proximal sesamoid bones and adjacent part of the intersesamoidean ligament to the distal fourth of the palmar surface of the proximal phalanx (Fig.1). The cruciate sesamoidean ligament included two bands of tissue located across the distopalmar recess of the joint. The fibers of each strand were attached proximally to the base of the respective proximal sesamoid bone and adjacent part of the intersesamoidean ligament. They extended obliquely towards the opposite palmar tubercle on the base of the proximal phalanx. The intersesamoidean ligament was represented by a narrow dense fibrocartilaginous mass which filled the space between the adjacent proximal sesamoid bones (Fig.1). The short sesamoidean ligaments consisted of short bands from the base of the proximal sesamoid bone to the palmar border of the base of the proximal phalanx (Fig.1). The related structures of fetlock joint included the superficial digital flexor tendon, the deep digital flexor tendon and the digital sheath which extended from above the fetlock joint to the middle of the middle phalanx. The sheath enclosed the deep digital flexor tendon, partially surrounding the superficial digital flexor tendon.

The joint capsule appeared to be capacious and attached around the articular surfaces consisting of fibrous and synovial layers. The capsule formed four recesses; two palmar or plantar and two dorsal recesses. The proximal-palmar recess was larger and the smaller one presented as a distodorsal recess. The dorsoproximal recess extended for 1.5-2cm on the third metacarpal bone (Fig.1). The small distodorsal recess (Figs.1,2+4) was narrow and a smaller section of the dorsal recess reached 2-3mm from the distal region to the articular surface of the first phalanx and related dorsally by the common digital extensor tendon and dorsolaterally by lateral extensor tendon. Access to the dorsal recess was possible both medially and laterally to the tendon of the long digital extensor muscle, the medial route was more accessible. The palmar recess had thin walls and was located between the distal extremity of third metacarpal bone and the suspensory ligament until its bifurcation; proximally, it was covered by the suspensory ligament, superficial and deep digital flexor tendons. The palmar recess formed a main palmaroproximal recess under the suspensory ligament, and a palmarodistal recess under the straight sesamoidean ligament and cruciate sesamoidean ligaments (Figs.1-4). The approach to the dorsal palmar recess was performed with the limb held in a flexed position and by palpating the triangle depression between suspensory ligament the third metatarcapal/tarsal bone and lateral proximal sesamoid bone.

3.2 Computed radiography

The dorsopalmar radiographs of the metacarpophalangeal and metatarsophalangeal joints were approximately symmetrical about the prominent sagittal ridge of the distal metacarpus, the medial condyle was slightly wider than the lateral. The sagittal ridge articulated with a groove in the proximal phalanx. The joint space was observed to be at right angles to the long axis of the third metacarpal bone. The proximal sesamoid bones superimposed on the third metacarpal/metatarsal bone and highlighted the axial and abaxial borders of the bone (Fig.2A). The dorsopalmar view allowed good visualization of the joint space and condyles of the distal third metacarpal/metatarsal. The lateromedial radiographs of the joints showed the condyles of the third metacarpal/metatarsal bone and proximal sesamoid bones superimposed on each other and the joint space was identifiable. The joint surface of the distal metacarpal/metatarsal condyle was smooth and curved. In the lateromedial view only the dorsal and palmar/plantar aspects were visualized (Fig.2B). The flexed lateromedial radiographs highlighted specific areas of the joint, especially the distal aspect of the sagittal ridge, which was less opaque and more dorsally located than the medial and lateral condyles, and elevated the proximal sesamoid bones away from the joint surface. It also enabled visualization of the dorsal-palmar and palmarodistal recesses of the joint (Fig.2C) and of the entire articular surfaces of the proximal sesamoid bones and of the sagittal ridge of the metacarpal/metatarsal bones in comparison to standard lateromedial and dorsopalmar projections. The dorsolateral-palmaromedial oblique and dorsomedial-palmarolateral oblique views highlighted the lateral sesamoid and dorsomedial aspects of the joint or medial sesamoid and dorsolateral aspects of the joint respectively.

In addition to showing the features of the normal limb, x-rays were used to investigate the non-healthy limbs in which new bone projections were extensive and radiodense growths varied in shape and size along the apical and basilar portions of the proximal sesamoid. Two cases of metacarpophalangeal joint sesamoiditis were accompanied by calcification of the suspensory ligament which appeared as mineralized opacities superimposed on suspensory ligaments (Fig.3A+B).

3.3 Computed tomography

The bone windows clarify the bone of the distal extremity of metacarpal and metatarsal bones, diaphysis and sagittal ridges of third metacarpal/metatarsal bones, the condyles, the proximal sesamoid bones and the proximal phalanx were seen on transverse and sagittal images (Fig.5+Supp Fig 2). All images had obvious delineation between the cortex and medulla of the bones and had smooth outlines and homogenous contours. The soft structures such as ligaments, tendons and synovial sheath were homogenously hypodense, visualization was difficult using this window. The soft tissue window with transverse and sagittal planes identified the common extensor tendon, dorsal extensor tendon, superficial digital flexor tendon, deep digital flexor tendon and digital sheath cavity (Fig. 5+Supp Fig 2), intersesamoidean ligament, straight and oblique sesamoidean ligaments. Medial and lateral branches of suspensory ligament were the same density as the intersesamoidean ligament and were difficult to recognize in this study and were therefore no discussed further.

Computed tomography at 120kV and 300mA: The bone window usage on the sagittal images showed a comprehensive evaluation of the sagittal ridge contour, proximal sesamoid bone and condyles of the two joint extremities (Supp Fig 2). All images showed excellent delineation between the cortex, medulla of bone and provided more detail about the bone density and thickness of the subchondral bone of the distal condyles of the third metacarpal/metatarsal bones (Fig.6). The soft tissue window with transverse and sagittal plans identified; suspensory ligament branches, extensor branches of the suspensory ligament, superficial and deep digital flexor tendons, common digital extensor tendon, straight, oblique, and cruciate sesamoidean ligaments, intersesamoidean ligament and the collateral ligaments (Fig.6 +Supp Fig 2) respectively. The proximal, distal synovial tendon sheath (the recesses of the digital sheath (cavity)) were best visualized on sagittal and transverse images, as a thin hypodense rim surrounding the deep digital flexor tendon (Fig.6+Supp Fig 2) and the four joint recesses were recognizable. Cruciate sesamoidean ligaments were evaluated better using a longitudinal rather than transverse view. Collateral sesamoidean ligaments and short sesamoidean ligaments could also be identified using transverse views (Fig.6).

3.4 Computed tomography of the abnormal metacarpophalangeal and metatarsophalangeal joints.

The usage of transverse computed tomography bone windows of the abnormal metacarpophalangeal joints at 120kV and 120mA at different levels of the sesamoid bone and dorsopalmar view showed a bony projection (bone exostosis) which was thin and curved medially. X-ray views made it difficult to determine positions and directions of the exostosis, whilst computed tomography bone window images gave more information enabling determination of the position and direction of even small/thin exostosis (Fig.7). The bony exostosis was observed in four of the five non-healthy donkeys.

Soft window transverse and sagittal computed tomography images were also used to look at the abnormal metatarsophalangeal joints at 120kV and 300mA (Fig.8). The soft window transverse computed tomography images of the abnormal metatarsophalangeal joint at the level proximal to, and at the level of, the sesamoid bone, show an increased joint cavity size and appearance of a hyperdense transverse septum. There was a septum presented at the palmar recess with obvious demarcation of synovial fluid (synovitis). There was an abnormal wave like shape appearance of the superficial digital extensor tendon, however this could have been an artifact due to dissection and should be studied in further in live animals. In addition, changes in density and appearance of the fluid at the suspensory apparatus were observed.

4. Discussion

The present study identified anatomical features in both the healthy and abnormal metacarpophalangeal and metatarsophalangeal joints in donkeys using complementary imaging techniques. The morphological structures of the articular surfaces within the metacarpophalangeal and metatarsophalangeal joints of the donkey and ligaments of the joints bear resemblances to those published in the literature about horses [16-18]. One major difference was that the donkey joint capsule formed a dorsal recess which had a large dorsal and small distodorsal recess, whilst the palmar or plantar recess consisted of dorsal-ventral parts, these structures have not been observed in the publications pertaining to the horse.

Radiographic exam is sensitive enough to identify consistent lesions with proliferative synovitis and osteoarthritis [19, 20] and is the most used imaging tools for the diagnosis of bone disorders affecting the metacarpophalangeal and metatarsophalangeal joints [1, 19, 21, 22]. The current study indicated the importance of flexed lateromedial radiographs giving better depictions of the articular surfaces of the proximal sesamoid bones and sagittal ridge of the metacarpal/metatarsal bone. This provided more accurate localization of lesions and better morphology of these structures, including osteochondritis of the distal sagittal ridge which has not previously been observed and/or erroneously diagnosed as cystic lesions [1, 22]. The lateromedial view allowed good visualization of the palmar/plantar aspect of condyles of the distal third metacarpal/metatarsal, base of the proximal sesamoid bones and first/proximal phalanx [19, 21]. The dorsopalmar view enabled good visualization of joint spaces and condyles of the distal third metacarpal/metatarsal bone. So most condylar fractures are best visualized on that projection revealing an abaxial and proximal displacement [19, 23]. The dorsolateral-palmaromedial and dorsomedial-palmolateral 45° oblique views allowed assessment of the shape, internal architecture and the apex, dorsal, palmar and distal borders of the lateral and medial proximal sesamoid bones respectively. It was also required to highlight individual proximal sesamoid bones because standard views allowed only partial visualization of these structures [21] (Fig.2D+E). The 45° oblique views were better for evaluating the regions of insertion of the suspensory ligament branch on the abaxial surface of the proximal sesamoid bone. It also allowed assessment of the medial and lateral palmar process of the proximal phalanx and the dorsomedial and dorsolateral aspects aspect of the joint respectively. Based on the results of the current study, it is recommended that intraarticular anesthesia/medication of the metacarpophalangeal and metatarsophalangeal joints in donkeys is performed via the three traditional approaches used in horses; the dorsal recess, palmar/plantar recess or through the collateral ligament of the proximal sesamoid bone. The latter approach is favored by most practitioners [24] and is performed with the limb held in a flexed position with the needle directed perpendicularly to the palpable depression between the third metatarcapal/tarsal bone and lateral proximal sesamoid bone at the level of proximal aspect of the collateral ligament of the joint.

Two chronic lesions with new bone proliferation, sesamoditis and calcification of suspensory ligament, were diagnosed using radiography and elicited a pain response on palpation. With four of the five unhealthy animals showing exostosis which was not observed in the healthy animals or described in the literature to date, this matter warrants further investigation. Whether these growths developed in response to limb complications or caused the lameness in these animals is yet to be established. It is possible they are secondary to chronic pathology in the digital sheath and some may reflect chronic tendon lesions which have mineralised. Differing theories in relation to inflammation, acute trauma, prolonged exposure to lameness, microfractures in the bone stimulating bone redevelopment and the extra bone growth itself increasing levels of lameness could all be possible reasons for the exostosis or lameness observed. There is a growing body of evidence to suggest that lameness is strongly associated with extra bone/cartilage proliferation and growth. Bovine lameness has been associated with extra bone growth on the caudal aspect of the distal phalanx [25] and on or around the flexor tuberosity with age [26]. Humans also have extra bone growth such as ‘bony spur formation’ and enthesopathy including calcification and irregular bone profiles in relation to activities such as increased mechanical load and exercise in addition to a number of limb, endocrine and metabolic disorders [27, 28]. Exostosis in horses has also been linked to lameness including on the metacarpal and metatarsal bones and the radius [29-31],

Computed tomography provided a comprehensive evaluation of the contour of the sagittal ridge, proximal sesamoid bone and condyles of two extremities forming the joint, especially using bone windows at 120kV and 300mA. Moreover, all images showed excellent delineation between the cortex, medulla of bone and provided more details about the thickness and bone density of the subchondral bone of the distal condyles of the third metacarpal/metatarsal bones. Several published studies discuss the superiority of computed tomography over the radiography for the diagnosis and understanding the underlying pathological change in osteoarthritis [32-34] condylar fracture [35, 36] and third metacarpal palmar condyle disease [34]. This superiority in the evaluation of the metacarpophalangeal and metatarsophalangeal joints is due to the complex anatomical arrangement of the joint with the superimposition of the sesamoid bones and the distal third metacarpal and first/proximal phalanx. Additionally computed tomography provided highly detailed cross-sectional and three-dimensional images, making it superior for some clinical evaluations.

Computed tomography evaluation of subchondral bone is crucial for early diagnosis of injury, and helps to explain the possible causes of lameness without classic clinical or radiographic changes or positive intraarticular blocking. Failure of intra-articular anesthesia to alleviate subchondral bone pain is problematic [37-40]. Cartilage damage has a later onset and the pain emanates from subchondral bone [41], 30-50% of the bone can be lost prior to it being identified radiographically [42, 43]. Therefore, computed tomography can yield better anatomic orientations of the subchondral bone and provide a more sensitive detection and characterization of osteolysis and osteogenesis than conventional radiographs and more importantly prior to clinically significant effects [42, 43]. This is also an important factor to consider when assessing exostosis as observed in the abnormal limbs in this study. The present study showed that CT images were more sensitive and comprehensive when detecting exostosis than conventional radiographs. The difficulties in showing exostosis specificity and severity in horses has been highlighted in previous studies using radiography and ultrasonography [31].

Details of the soft tissue in computed tomography have previously been inferior to magnetic resonance imaging [16, 44]. The present study highlighted that in addition to bone structures being observed, clinically important soft tissue structures may be identified better by adjusting the tube current to 300mA instead of 120mA, however further studies are required to fully investigate this. With image thickness and kilovoltage held constant, a reduction in tube current increases image noise but decreases radiation exposure, so there is a tradeoff between image quality and radiation dosage [45]. Likewise, increasing tube current leads to increased radiation exposure and decreased image noise, but lesions may be obscured by higher noise levels [46-49]. It has also been reported that ‘image noise’ can be improved by using a higher tube current, because it is inversely proportional to the square root of the photon flux [7]. Consistent with these theories, the contrast-to-noise ratio and the confidence level of low-contrast phantom detection were enhanced by increasing tube voltage and tube current. With section thickness set at 10mm, the contrast-to-noise ratio increased from 0.8 obtained at 400mAs and 120kVp, to 1.0 at a tube current and voltage of 450mAs and 135kVp, respectively. However irradiation doses increase with current increases therefore caution is advised in the clinical setting, highlighting an area of future research. Future research expanding the number of donkeys and the types of limb disorders, which were limitations of the study, would also benefit this area. A full investigation into the types and locations of the exostosis in differing limb disorders would enhance the knowledge about the types of abnormalities and potentially inform diagnosis and treatment in addition to under the basic biological mechanisms underlying the exostosis. This would include the use of imaging techniques but also histological and molecular and cellular techniques in order to fully understand the mechanisms behind the growth. As the horse is so closely related to the donkey, a comparative study of the two animals would provide a unique insight into lameness disorders.

5. Conclusions

This study has shown the anatomy of the normal and lameness affected metacarpophalangeal and metatarsophalangeal joints in the donkey, identified differences between the structures and highlighted clinically important information in relation to potential sites of injection and imaging. This included not only new anatomical structures but also exostosis which was present in animals with a history of lameness but not in those with healthy limbs. Anatomical knowledge is essential not only for present clinical procedures but also for emerging treatments including gene therapy [50]. We have also shown that optimized computed tomography enabled more precise evaluation of bone lesions and metacarpophalangeal and metatarsophalangeal joint adjacent structures and developed of protocols for clinical and research practice.

Conflict of Interest:
Declarations of interest: none

List of Author Contributions
Samir A.A. El-Gendy: Conception and Design, Acquisition of Data, Analysis and Interpretation of Data, Drafting the Article, Revising Article for Intellectual Content, Final Approval of the Completed Article. **Mohamed A.M. Alsafy**: Analysis and Interpretation of Data, Drafting the Article, Final Approval of the Completed Article. **Catrin S. Rutland:** Analysis and Interpretation of Data, Drafting the Article, Revising Article for Intellectual Content, Final Approval of the Completed Article. **Ahmad N. EL-Khamary:** Acquisition of Data, Analysis and Interpretation of Data, Drafting the Article, Final Approval of the Completed Article. **Howaida M. Abu-Ahmed:** Acquisition of Data, Analysis and Interpretation of Data, Drafting the Article, Final Approval of the Completed Article. **Mahmoud H. El-Kammar:** Conception and Design, Acquisition of Data, Analysis and Interpretation of Data, Drafting the Article, Revising Article for Intellectual Content, Final Approval of the Completed Article.

Acknowledgements
Funding was kindly provided by Alexandria University, Damanhur University and The University of Nottingham. Funding sources had no other involvement in the study.

[1] Machado VMV, Aguiar ACS, Viana GF, Crosignani NO, Puoli JNP. Diagnostic value of computed tomography, radiography and ultrasonography in metacarpophalangeal joint disorders in horses. Arq Bras Med Vet Zoo. 2016;68:66-72.
[2] Ross MW, Dyson SJ. Diagnosis and management of lameness in the horse. Philadelphia, USA.: Elsevier-Saunders.; 2003.
[3] Amin M, Elbakary RMA, Alsafy MAM, Fathi n. Radiographic and Computed Tomographic Anatomy of the Fetlock, Pastern and Coffin joints of the Manus of the Donkey (Equus asinus). Alexandria J Vet Sci. 2014;41:68-79.
[4] Badawy M. Computed Tomographic Anatomy of the Fore Foot in One-Humped Camel. Glob Vet. 2011;6:417-23.
[5] Groth AM, May SA, Weaver MP, Weller R. Intra- and interobserver agreement in the interpretation of navicular bones on radiographs and computed tomography scans. Equine Vet J. 2009;41:124-9.
[6] Widmer WR, Buckwalter KA, Fessler JF, Hill MA, VanSickle DC, Ivancevich S. Use of radiography, computed tomography and magnetic resonance imaging for evaluation of navicular syndrome in the horse. Vet Radiol Ultrasoun. 2000;41:108-16.
[7] Tanaka C, Ueguchi T, Shimosegawa E, Sasaki N, Johkoh T, Nakamura H, et al. Effect of CT acquisition parameters in the detection of subtle hypoattenuation in acute cerebral infarction: a phantom study. AJNR Am J Neuroradiol. 2006;27:40-5.

[8] Swai ES, Bwanga SJR. Donkey keeping in northern Tanzania: socio-economic roles and reported husbandry and health constraints. Livestock Res Rural Dev. 2008;20:1-97.
[9] Wilson RT. The past, present and future of domestic equines in Tanzania. J Equine Sci. 2013;24:37-45.
[10] McKenna C. Bearing a Heavy Burden. London, UK.: The Brooke.; 2007.
[11] Waltraud K., Grunenfelder HP, Broxham E. Donkey Breeds in Europe: Inventory,. St.Gallen, Switzerland: Monitoring Institute for Rare Breeds and Seeds in Europe; 2008.
[12] Elmesiry A., Seleim M, Cullis-Hill D. Iodoacetate and allogenous cartilage particles as models for arthritis induction in equine. Int J Vet Sci Med. 2014;2:142-50.
[13] Mokbel AN, El Tookhy OS, Shamaa AA, Rashed LA, Sabry D, El Sayed AM. Homing and reparative effect of intra-articular injection of autologus mesenchymal stem cells in osteoarthritic animal model. BMC Musculoskelet Disord. 2011;12:259.
[14] Singh KI, Sobti VK, Roy KS. Gross and histomorphological effects of therapeutic ultrasound (1 WATT/CM2) in experimental acute traumatic arthritis in donkeys. J Equine Vet Sci. 1997;17:150-5.
[15] (I.C.V.G.A.N) ICoVGAN. Nomina Anatomica Veterinaria. 6th ed: WAVA; 2017.
[16] Vanderperren K, Ghaye B, Snaps FR, Saunders JH. Evaluation of computed tomographic anatomy of the equine metacarpophalangeal joint. Am J Vet Res. 2008;69:631-8.
[17] Dyce KM, Sack WO, Wensing CJG. Textbook of veterinary anatomy: Elsevier Health Sciences; 2009.
[18] Gottschalk R. The equine distal limb: An atlas of clinical anatomy and comparative imaging (7th impression). J S Afr Vet Assoc. 2011;82:253.
[19] Vanderperren K, Saunders JH. Diagnostic imaging of the equine fetlock region using radiography and ultrasonography. Part 2: The bony disorders. Vet J. 2009;181:123-36.
[20] Park RD. Optimal radiographic views for evaluating thoroughbred yearlings - quality control of the radiographic image. 46th Annual Convention of the American Association of Equine Practitioners San Antonio, Texas, USA. 2000. p. 357-8.
[21] Butler JA, Colles CM, Dyson SJ, Kold SE, Poulos PW. Clinical Radiology of the Horse. 3rd. ed. Oxford, UK.: Blackwell Science; 2011.
[22] Wright IM, Minshall GJ. Identification and treatment of osteochondritis dissecans of the distal sagittal ridge of the third metacarpal bone. Equine Vet J. 2014;46:585-8.
[23] Vanderperren K, Saunders JH. Diagnostic imaging of the equine fetlock region using radiography and ultrasonography. Part 1: Soft tissues. Vet J. 2009;181:111-22.
[24] Misheff MM, Stover SM. A comparison of two techniques for arthrocentesis of the equine metacarpophalangeal joint. Equine Vet J. 1991;23:273-6.
[25] Newsome R, Green MJ, Bell NJ, Chagunda MGG, Mason CS, Rutland CS, et al. Linking bone development on the caudal aspect of the distal phalanx with lameness during life. J Dairy Sci. 2016;99:4512-25.
[26] Tsuka T, Ooshita K, Sugiyama A, Osaki T, Okamoto Y, Minami S, et al. Quantitative evaluation of bone development of the distal phalanx of the cow hind limb using computed tomography. J Dairy Sci. 2012;95:127-38.
[27] Benjamin M, Toumi H, Ralphs JR, Bydder G, Best TM, Milz S. Where tendons and ligaments meet bone: attachment sites ('entheses') in relation to exercise and/or mechanical load. J Anat. 2006;208:471-90.
[28] Slobodin G, Rozenbaum M, Boulman N, Rosner I. Varied presentations of enthesopathy. Semin Arthritis Rheum. 2007;37:119-26.

[29] Bertoni L, Forresu D, Coudry V, Audigie F, Denoix JM. Exostoses on the palmar or plantar aspect of the diaphysis of the third metacarpal or metatarsal bone in horses: 16 cases (2001-2010). J Am Vet Med Assoc. 2012;240:740-7.
[30] Zubrod CJ, Schneider RK, Tucker RL. Use of magnetic resonance imaging to identify suspensory desmitis and adhesions between exostoses of the second metacarpal bone and the suspensory ligament in four horses. Javma-J Am Vet Med A. 2004;224:1815-+.
[31] Zetterstrom SM, Johansson BC, Carmalt JL. Evaluation of clinical and tenoscopic findings in the carpal flexor sheath of horses. Am J Vet Res. 2017;78:840-6.
[32] Messent EA, Ward RJ, Tonkin CJ, Buckland-Wright C. Tibial cancellous bone changes in patients with knee osteoarthritis. A short-term longitudinal study using Fractal Signature Analysis. Osteoarthr Cartilage. 2005;13:463-70.
[33] Messent EA, Ward RJ, Tonkin CJ, Buckland-Wright C. Cancellous bone differences between knees with early, definite and advanced joint space loss; a comparative quantitative macroradiographic study. Osteoarthr Cartilage. 2005;13:39-47.
[34] Muir P, Peterson AL, Sample SJ, Scollay MC, Markel MD, Kalscheur VL. Exercise-induced metacarpophalangeal joint adaptation in the Thoroughbred racehorse. J Anat. 2008;213:706-17.
[35] Delguste C, Amory H, Guyonnet J, Thibaud D, Garnero P, Detilleux J, et al. Comparative pharmacokinetics of two intravenous administration regimens of tiludronate in healthy adult horses and effects on the bone resorption marker CTX-1. J Vet Pharmacol Ther. 2008;31:108-16.
[36] Dore F, Filippi L, Biasotto M, Chiandussi S, Cavalli F, Di Lenarda R. Bone scintigraphy and SPECT/CT of bisphosphonate-induced osteonecrosis of the jaw. J Nucl Med. 2009;50:30-5.
[37] Dyson S. Problems associated with the interpretation of the results of regional and intra-articular anaesthesia in the horse. Vet Rec. 1986;118:419-22.
[38] Niv D, Gofeld M, Devor M. Causes of pain in degenerative bone and joint disease: a lesson from vertebroplasty. Pain. 2003;105:387-92.
[39] Sampson SN, Schneider RK, Tucker RL, Gavin PR, Zubrod CJ, Ho CP. Magnetic resonance imaging features of oblique and straight distal sesamoidean desmitis in 27 horses. Vet Radiol Ultrasound. 2007;48:303-11.
[40] Schumacher J, Schramme MC, Schumacher J, DeGraves FJ. Diagnostic analgesia of the equine digit. Equine Vet Educ. 2013;25:408-21.
[41] Ross MW. Subchondral Bone Pain – The Fetlock Joint in Racehorses and Sports Horses. American Association of Equine Practitioners Orlando, USA. 2016. p. 58-64.
[42] Young BD, Samii VF, Mattoon JS, Weisbrode SE, Bertone AL. Subchondral bone density and cartilage degeneration patterns in osteoarthritic metacarpal condyles of horses. Am J Vet Res. 2007;68:841-9.
[43] Schramme M, Schumacher J, Schumacher J. Clinical examination, differential analgesia and imaging modalities for the investigation of distal limb lamness. Lameness and Imaging - American Association of Equine Practitioners Focus Meeting. Fort Collins, Colorado, USA. 2007. p. 51-69.
[44] Bienert A, Stadler P. Computed tomographic examination of the locomotor apparatus of horses - a review. Pferdeheilkunde. 2006;22:218.
[45] Nsoor N. Factors That Can Be Attributable to Radiation Dose Reduction among Pediatric Age Group Undergoing Brain Computed Tomography. Pak J Med Sci. 2009;25:669-73.
[46] Kalra MK, Blake MA, Maher MM. Does low dose abdominal-pelvic CT compromise the lesion detection and morphological appearance? Am J Roentgenol. 2003;180:8.

[47] Kalra MK, Maher MM, Toth TL, Schmidt B, Westerman BL, Morgan HT, et al. Techniques and applications of automatic tube current modulation for CT. Radiology. 2004;233:649-57.
[48] Li F, Sone S, Abe H, MacMahon H, Armato SG, Doi K. Lung cancers missed at low-dose helical CT screening in a general population: Comparison of clinical, histopathologic, and imaging findings. Radiology. 2002;225:673-83.
[49] Rehani MM, Bongartz G, Kalender W, Golding SJ, Gordon L, Murakami T, et al. Managing x-ray dose in computed tomography: ICRP special task force report. Ann ICRP 2000:7-45.
[50] Kovac M, Litvin YA, Aliev RO, Zakirova EY, Rutland CS, Kiyasov AP, et al. Gene Therapy Using Plasmid DNA Encoding Vascular Endothelial Growth Factor 164 and Fibroblast Growth Factor 2 Genes for the Treatment of Horse Tendinitis and Desmitis: Case Reports. Front Vet Sci. 2017;4:168.

Table 1. Donkey Specimens

Donkey identification number	**Age (years)**	**Sex**	**Condition**	**X-ray**	**Computed tomography**	**Anatomical dissection and cast**
1	5	Male	Healthy	X	X	
2	5	Male	Healthy	X	X	X
3	8	Female	Healthy	X		X
4	7	Female	Healthy	X		
5	7	Male	Healthy	X		
6	7	Male	Affected	X	X	
7	5	Male	Affected	X	X	
8	5	Male	Affected	X	X	
9	7	Female	Affected	X	X	
10	8	Female	Affected	X	X	
11	5	Male	Healthy			X
12	6	Male	Healthy			X
13	7	Male	Healthy			

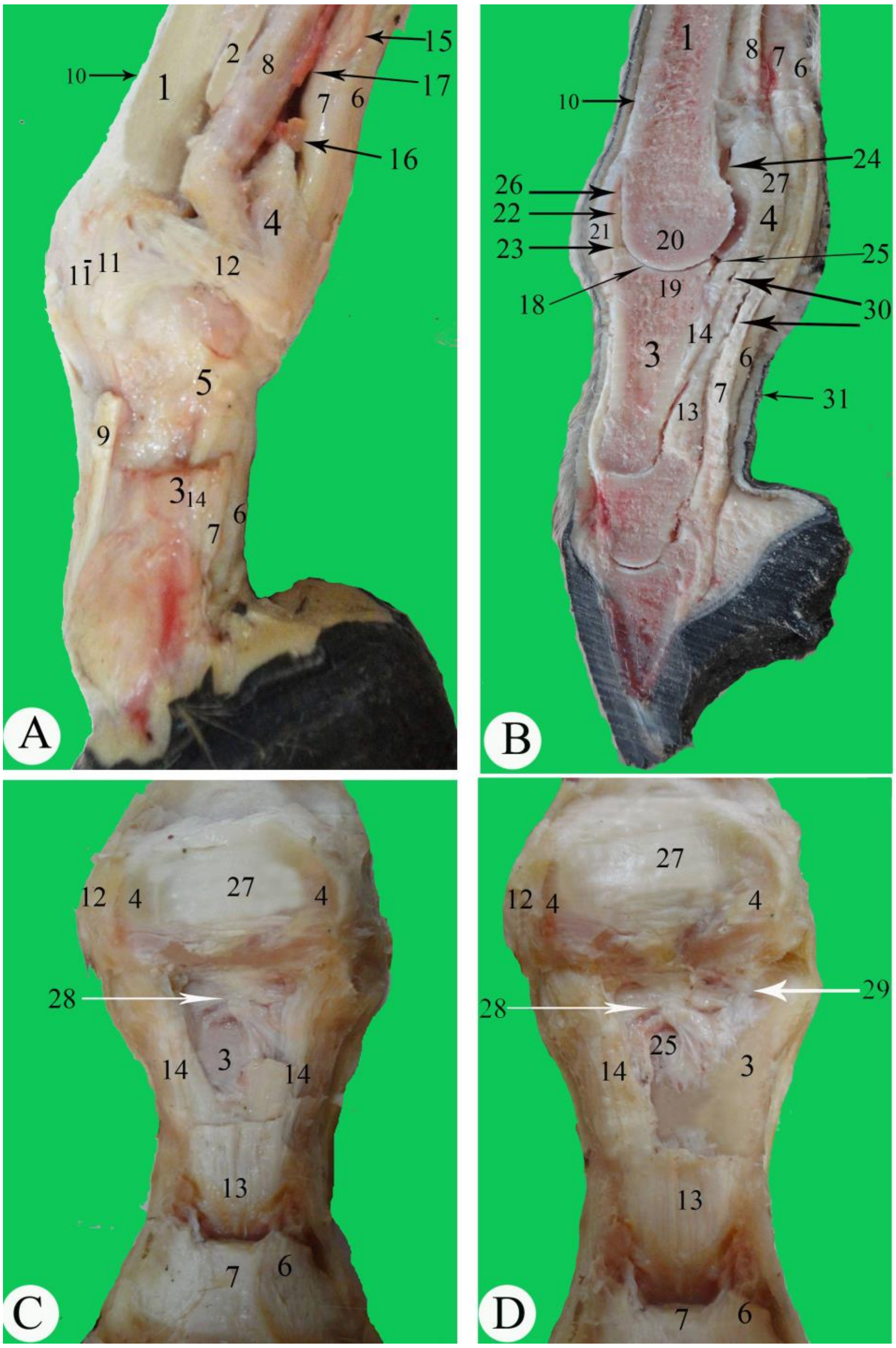

Fig.1. Anatomical dissection of metatarsophalangeal joint. (A) Medial, (B) sagittal and (C-D) plantar views. 1-Third metatarsal bone. 2-Second metatarsal bone. 3-Proximal phalanx. 4-Proximal sesamoid bone. 5-Proximal digital annular ligament. 6-Superficial digital flexor tendon. 7-Deep digital flexor tendon. 8-Suspensory ligament. 9-Extensor branch of suspensory (dissected). 10-Long digital extensor tendon. 11-Collateral ligament of the joint (superficial+deep). 12-Medial collateral sesamoidean ligament. 13-Straight sesamoidean ligament. 14-Oblique sesamoidean ligament. 15-Medial plantar nerve. 16-Lateral dorsal metatarsal artery. 17-Plantar vein. 18-Joint cavity. 20-Metatarsal condyle. 21-Dorsal capsule of the joint. 22-Dorsal recess. 23-Distodorsal recess. 24-Proximal plantar recess. 25-Distal plantar recess. 26-Plica synovialis. 27-Intersesamoidean ligament. 28-Cruciate sesamoidean ligaments. 29-Short sesamoidean ligament. 30-Synovial digital sheath cavity. 31-Skin.

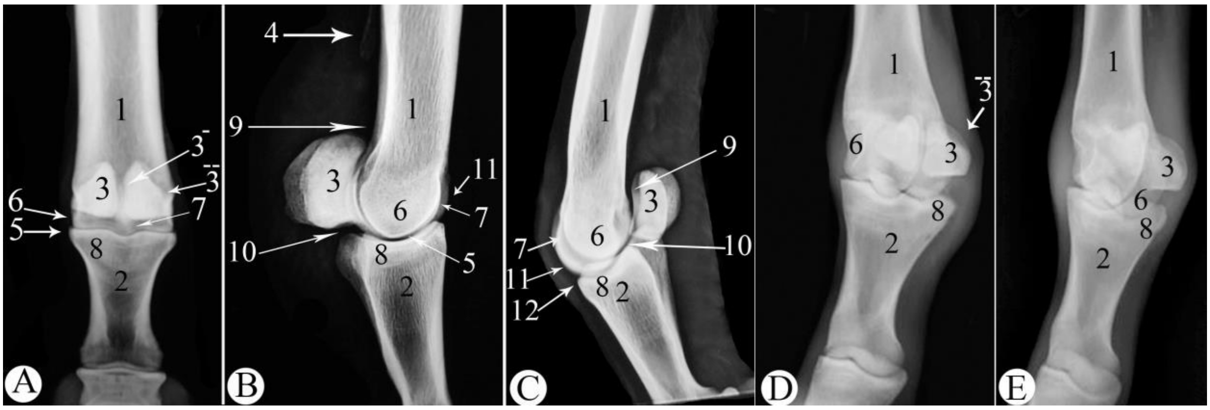

Fig. 2. Normal radiographic appearance of the metacarpophalangeal joint; (A) Dorsopalmar, (B) Lateromedial, (C) Oblique flexed lateromedial, (D) Dorsolateral-palmaromedial oblique, (E) Dorsomedial-palmarolateral oblique. 1-Third metacarpal bone. 2-Proximal phalanx. 3-Proximal sesamoid bone. 3^{a}axial border. 3^{b}abaxial border. 4-Second/fourth metacarpal bone. 5-Joint cavity. 6+7-Condyle of the third metacarpal bone. 9-proximal-palmar recess. 10-Distal-palmar recess. 11-Dorsal recess. 12-Distodorsal recess.

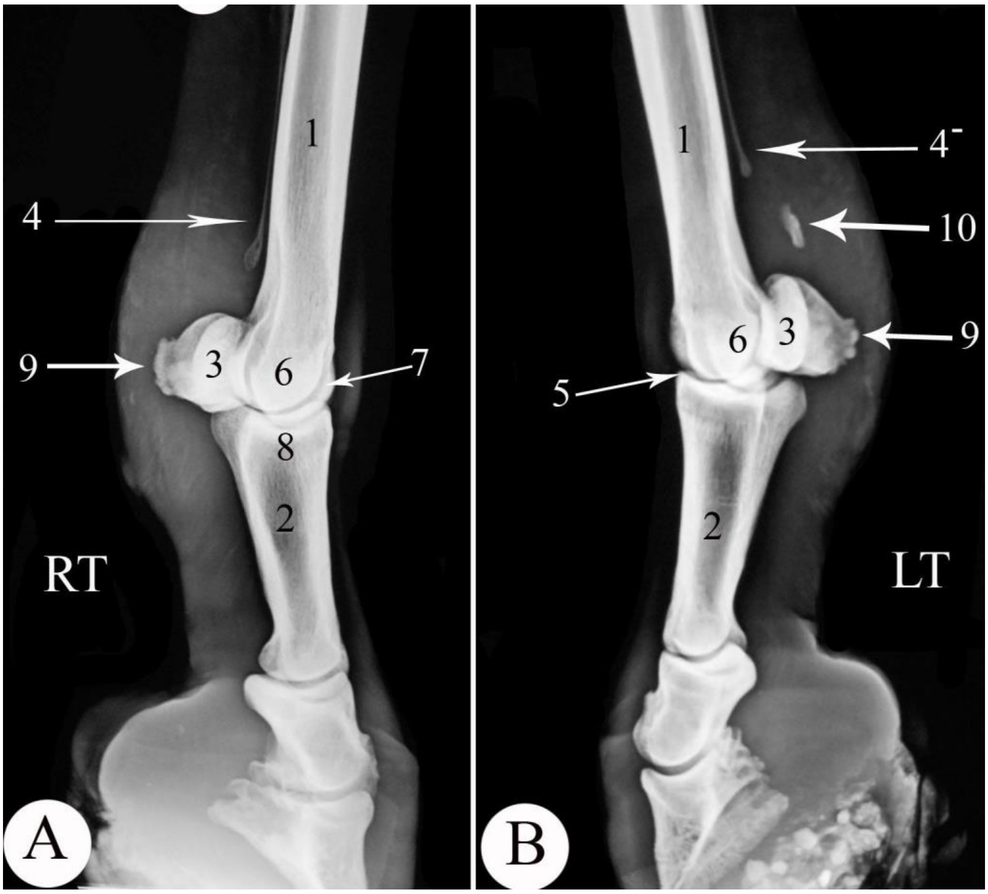

Fig. 3. New bone proliferations on the palmar margin of the proximal sesamoid bones and calcification of the lateral branch of the suspensory ligament. Oblique views of right (A) and left (B) metacarpophalangeal joint; 1-Third metacarpal bone. 2-Proximal phalanx. 3-Proximal sesamoid bone. 4 and 4- -Second and fourth metacarpal bone, cannot be differentiated given the view. 5-Joint cavity. 6-Condyles of third metacarpal. 7-Sagittal crest. 9-Bony exostosis. 10-Calcification of suspensory ligament lateral branch.

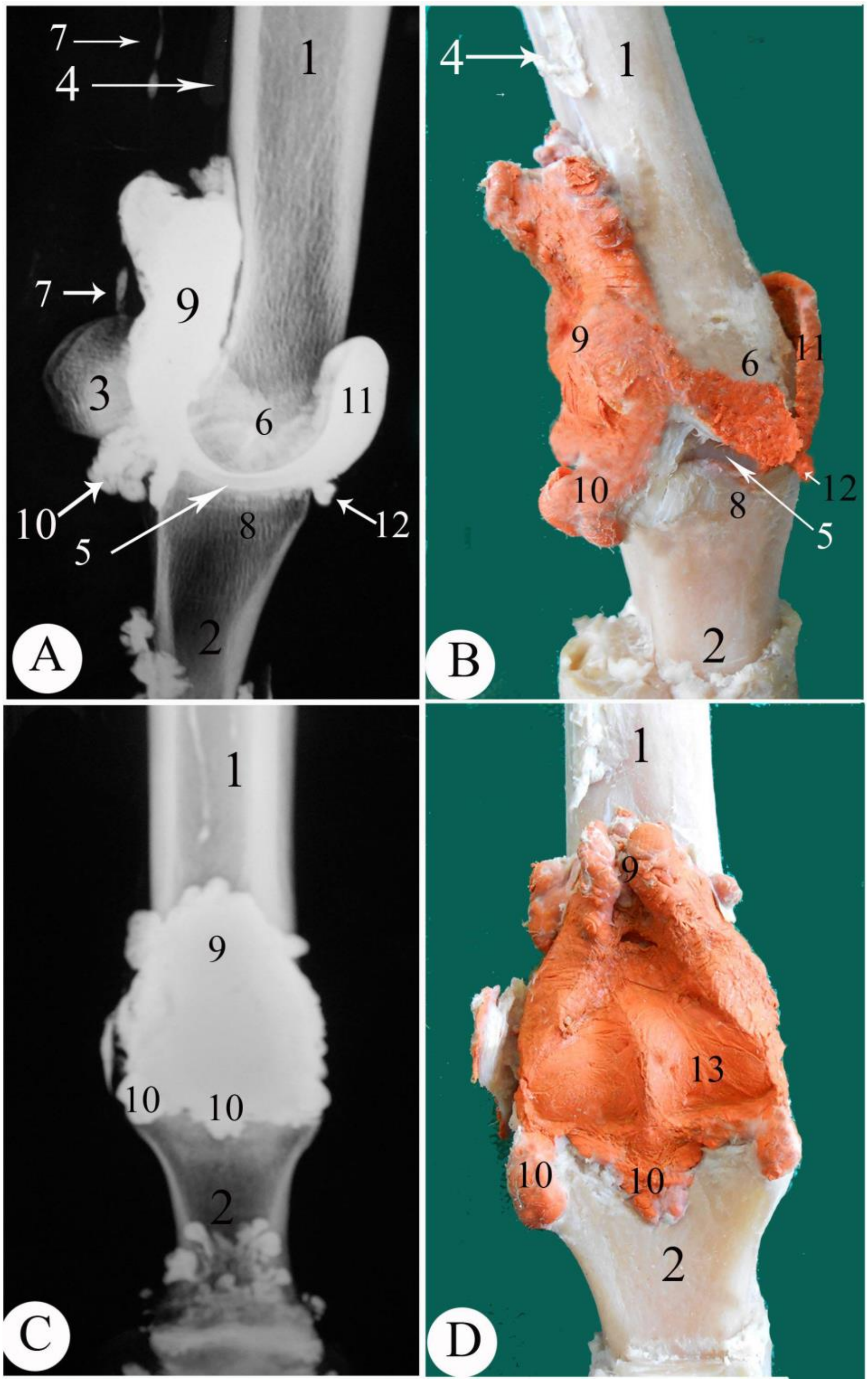

Fig. 4. Contrast radiographic and dissected cast images of the metacarpophalangeal joint, possibly with a distended joint and marked synovial proliferations. . (A) Lateromedial contrast radiograph. (B) Lateral view of dissected cast. (C) Dorsopalmar contrast radiograph. (D) Palmar view of dissected cast. 1-Third metacarpal bone. 2-Proximal phalanx. 3-Proximal sesamoid bone. 4-Distal end of the second metacarpal bone 5-Joint cavity. 6-Condyle of metacarpal. 7-Digital sheath or possible mineralization of the tendon. 9-Proximal-palmar recess. 10-Distal-palmar recess. 11-Dorsal recess. 12-Distodorsal recess. 13-Impression of proximal part of the sesamoid bone.

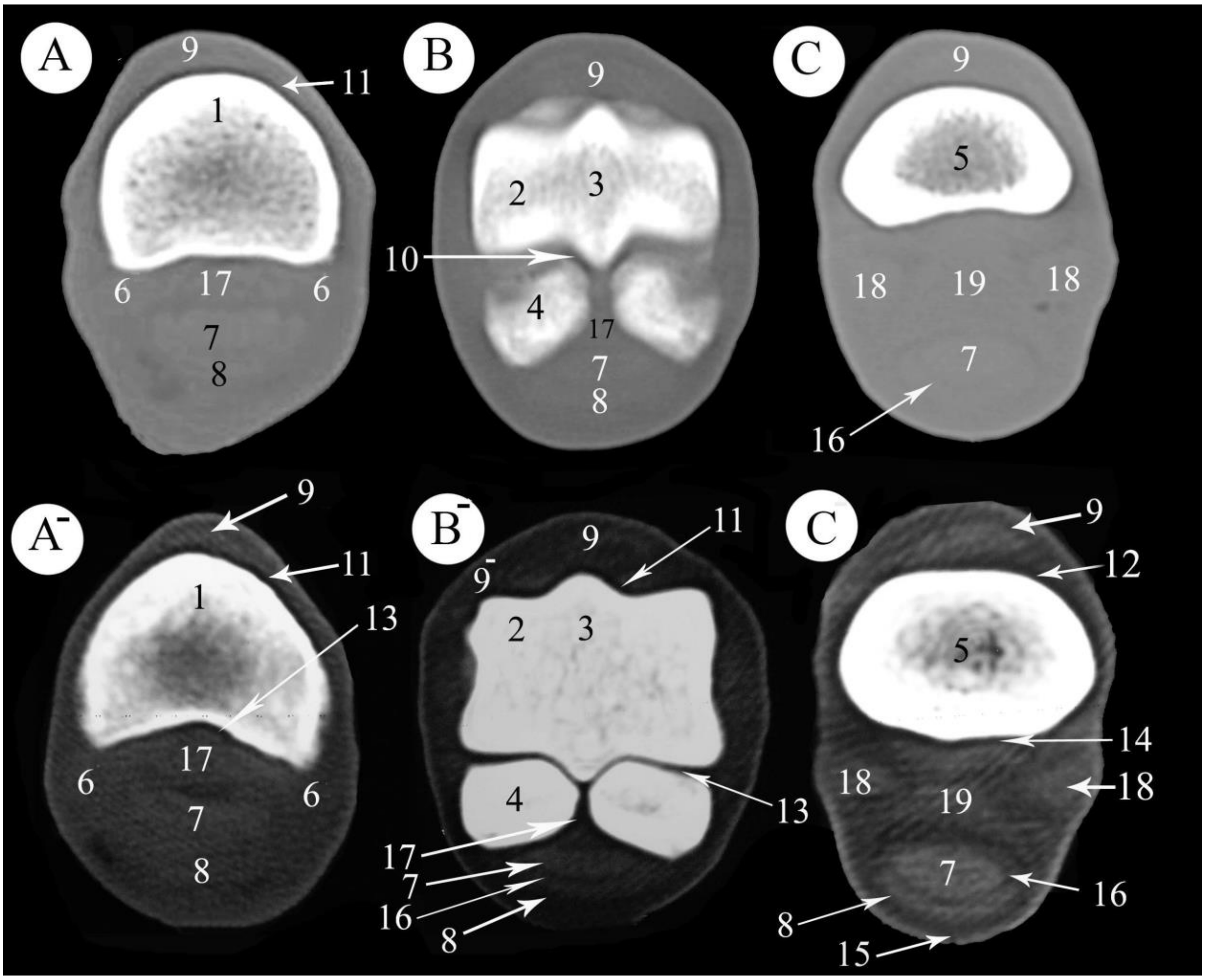

Fig. 5. Transverse computed tomography of the normal metacarpophalangeal joint at 110kV, 120mA. At the levels A) proximal to sesamoid bone, B) sesamoid bone, C) distal to sesamoid bone.

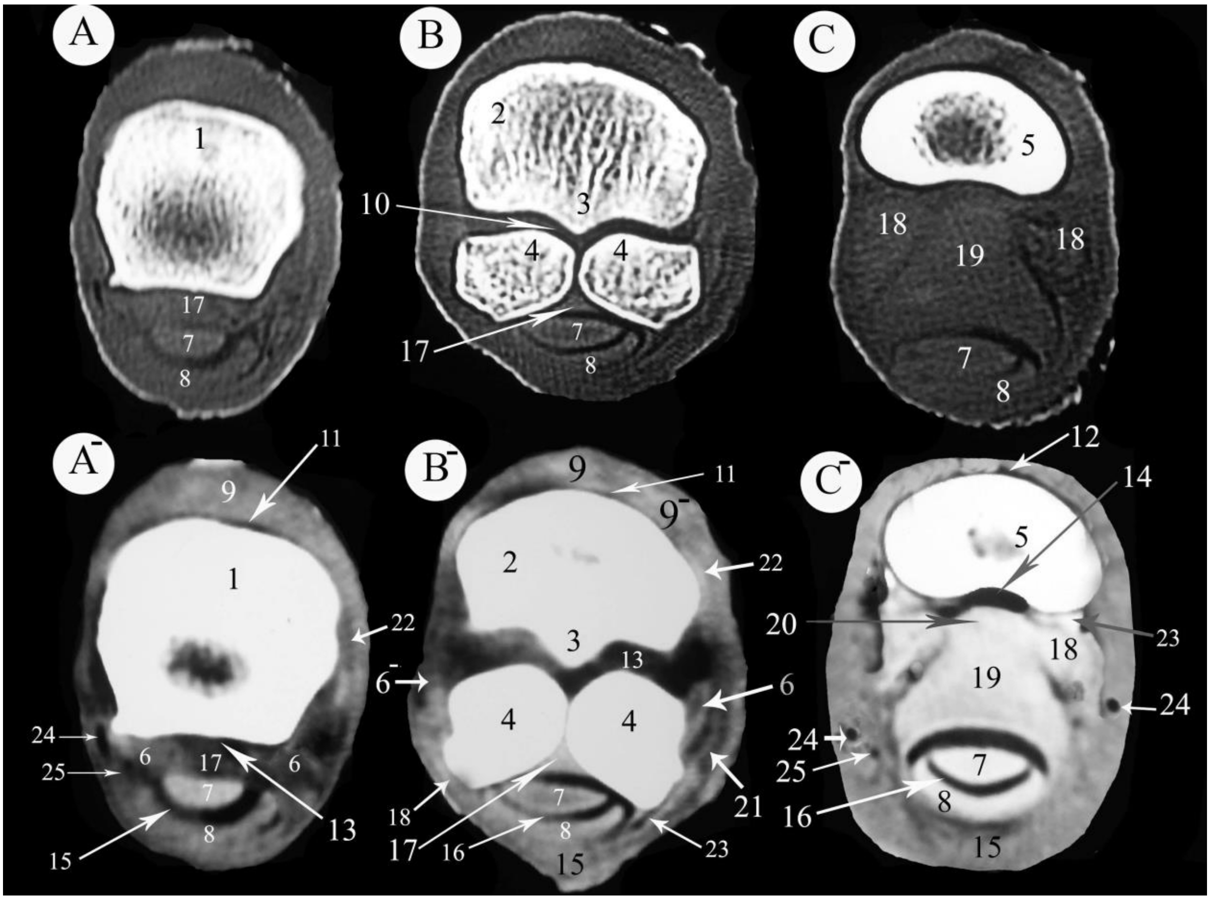

Fig. 6. Transverse Computed tomography of healthy metacarpophalangeal joint at 120kV, 300mA. Level A) proximal to sesamoid bone, B) sesamoid bone, C) distal to sesamoid bone.

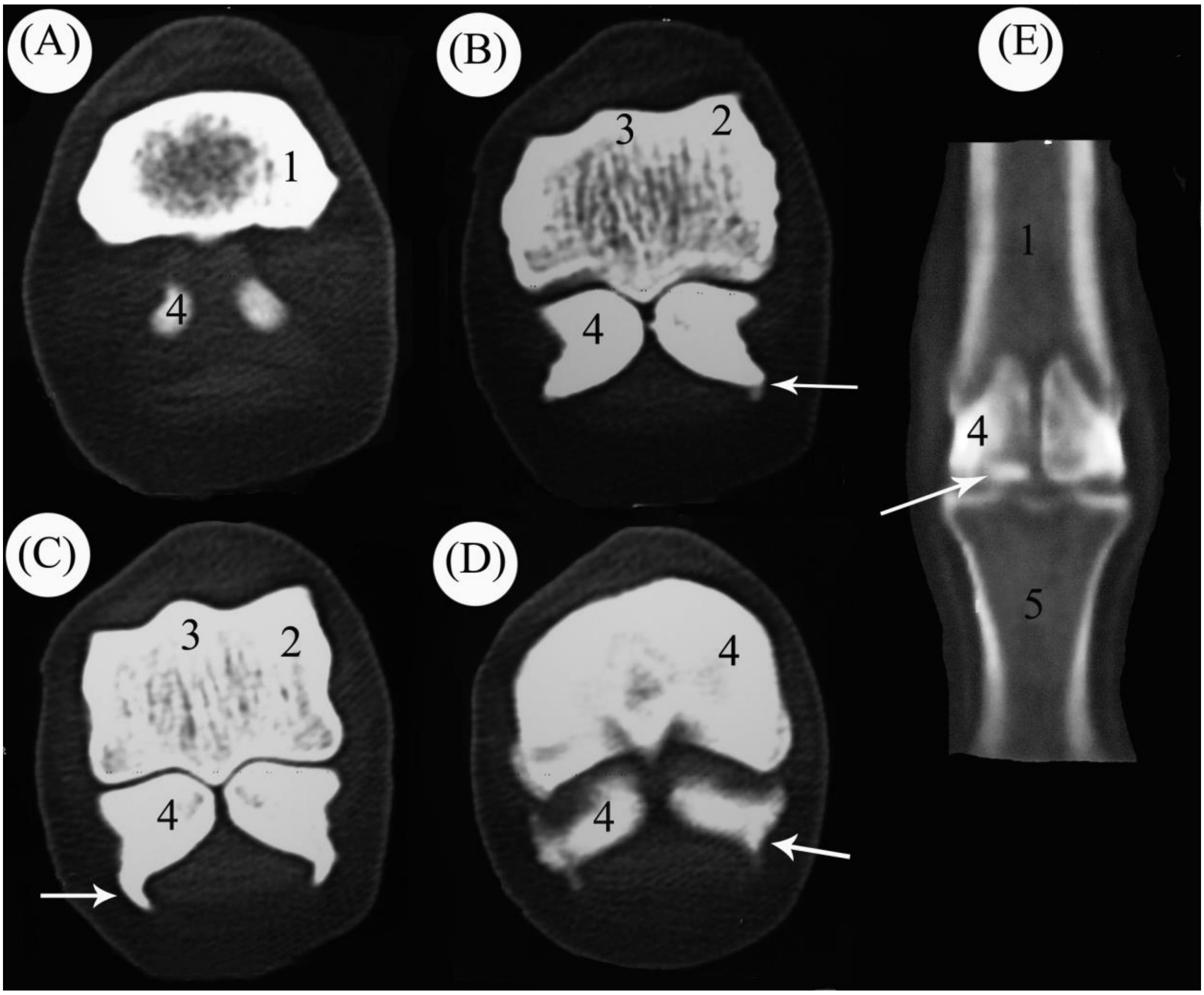

Fig. 7. Computed tomography of abnormal metacarpophalangeal joint from a transverse view (A-D) and dorsopalmar view radiograph (E) showing the bony projection (exostosis). 1-Third metacarpal bone. 2-Condyle of third metacarpal bone. 3-Sagittal ridge of third metacarpal bone. 4-Proximal sesamoid bone. 5-Proximal phalanx and bony extension (arrow).

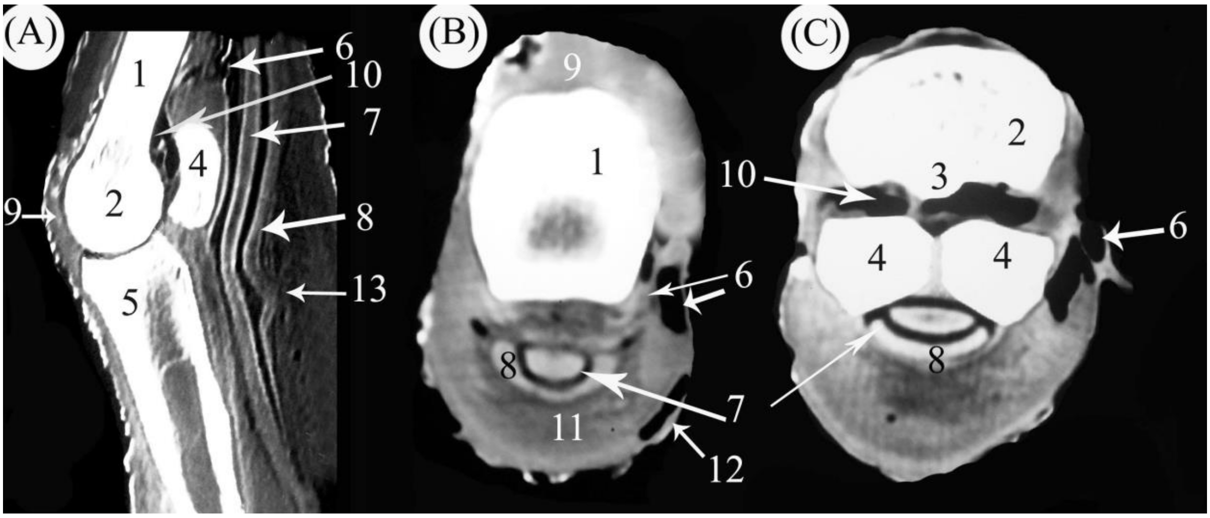

Fig. 8. Computed tomography of the abnormal metatarsophalangeal joint. Sagittal (A) and transverse views (B and C) soft window at 120kV, 300mA. At levels B) distal to the fetlock C) at sesamoid bone. 1-Third metacarpal bone. 2-Condyle of third metacarpal bone. 3-Sagittal ridge of third metacarpal bone. 4-Proximal sesamoid bone. 5-Proximal phalanx. 6-Note change of density and appearance of gas), 7-Deep digital flexor tendon. 8-Superficial digital flexor tendon. 9-Dorsal digital extensor tendon. 10-Joint cavity (note increase in size, appearance of hyperdense septa or structures). 11-Ergot cushion. 12-Fluid at the lateral part of the cushion. 13-Sigmoid shape of superficial digital flexor tendon.

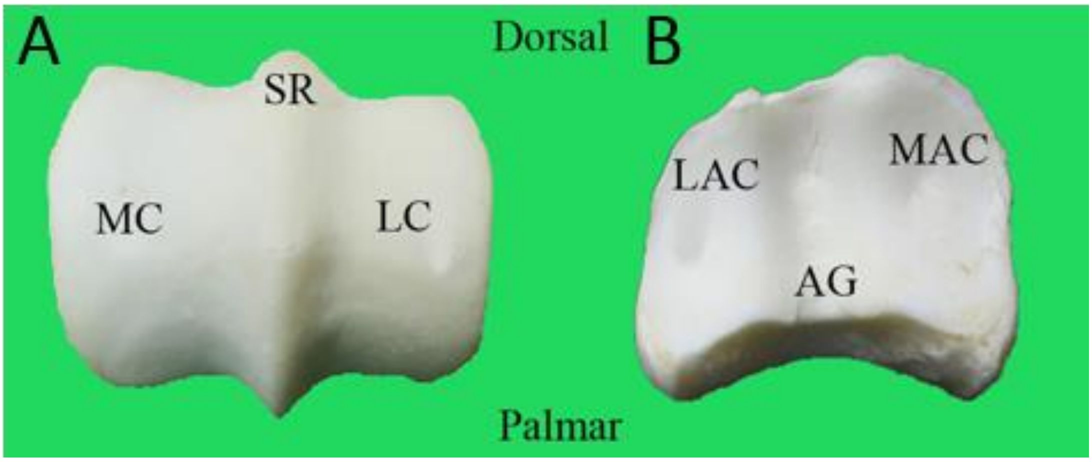

Supplemental Figure 1. Anatomical bone specimen. A) Distal extremity of third metacarpal bone. MC-medial condyle. LC-lateral condyle. SR-sagittal ridge. B) Proximal extremity of proximal phalanx. MAC-medial articular cavity. AG-sagittal groove. LAC-lateral articular cavity.

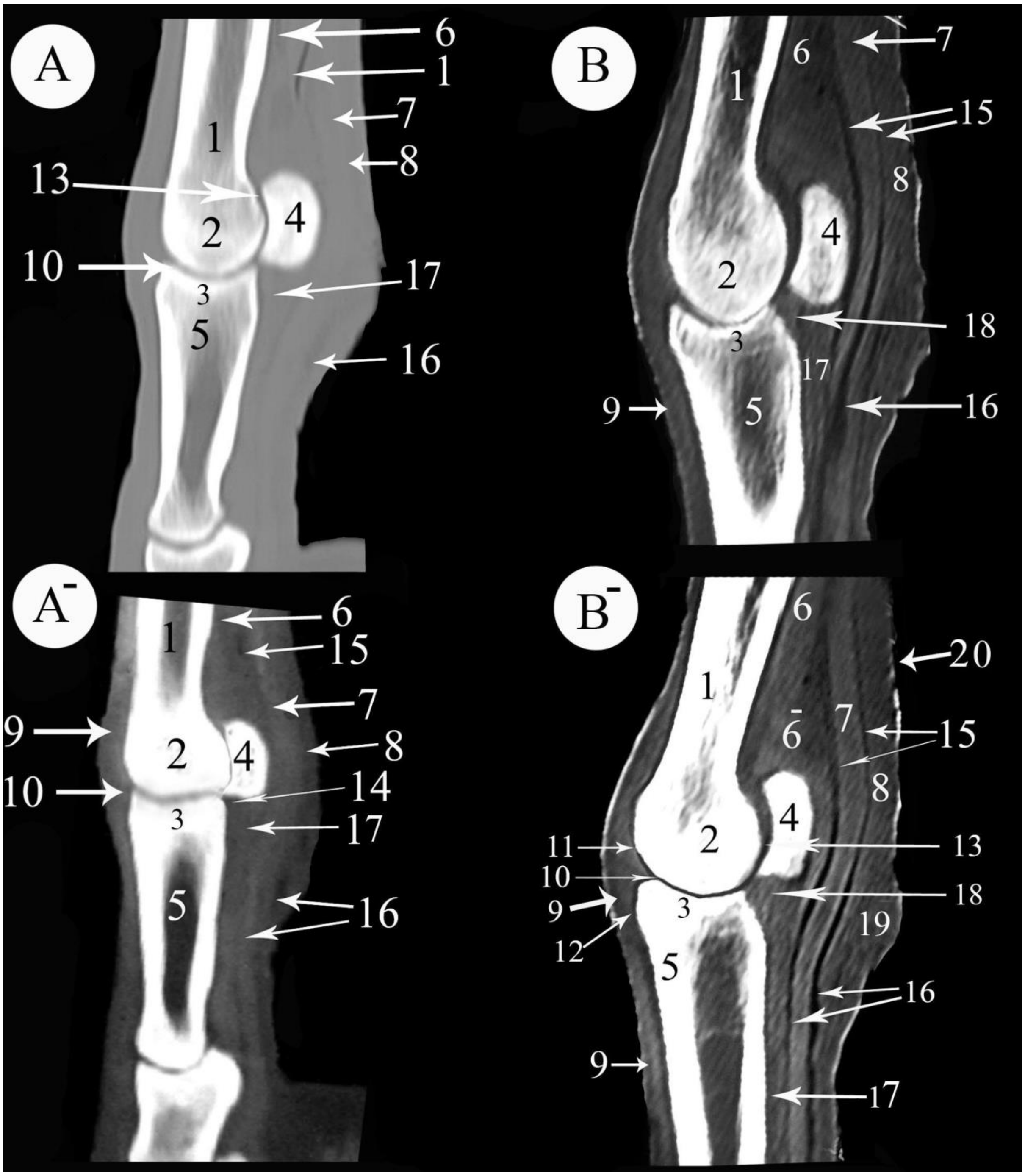

Supplemental Figure 2. Parasagittal Computed tomography of the normal metacarpophalangeal joint. A+B) are bone window and A^{-}+B^{-}) are soft window. (A +A^{-}) at 120kV, 120mA, while B+ B^{-}) 120kV, 300mA. 1-Third metacarpal bone. 2-Condyle of 3rd metacarpal bone. 3-Areticular cavity of proximal phalanx. 4-Proximal sesamoid bone. 5-Proximal phalanx. 6-Suspensory ligament. 6^{-}Branches of suspensory ligaments. 7-Deep digital flexor tendon. 8-Superficial digital flexor tendon. 9-Common digital extensor tendon.10-Joint cavity. 11-Dorsal recess. 12-Distodorsal recess. 13-Palmaroproximal recess. 14-Palmarodistalrecess. 15-Proximal digital sheath cavity. 16-Distal digital sheath cavity. 17-Straight sesamoidean ligament. 18- Cruciate sesamoidean ligaments. 19- Ergot cushion. 20-Skin.